Environmental Science
Water Research & Technology

PAPER

View Article Online
View Journal | View Issue

Cite this: *Environ. Sci.: Water Res. Technol.*, 2026, **12**, 168

The synergy between particles and biofilms that drives drinking water discolouration processes in PVC pipes

Artur Sass Braga, * Yves Filion and Benjamin Anderson

Received 18th September 2025,
Accepted 30th October 2025

DOI: 10.1039/d5ew00913h

rsc.li/es-water

This study investigates how biofilms influence the accumulation and mobilization of iron oxide particles in drinking water distribution systems (DWDSs). Two experiments were conducted in a full-scale PVC pipe loop: one with biofilms grown over 28 days and one without biofilms. Iron oxide particles were injected into the pipes under steady flow conditions to promote particle attachment to the pipe walls, followed by four sequential flushing steps designed to mobilize the attached particles. Particle accumulation and mobilization were assessed using suspended sediment concentration (SSC), turbidity, and microscopy. Biofilms increased particle attachment from 66% to 72% and enhanced particle retention during flushing. In the first flush, 79% of the mobilized mass was released in the no-biofilm loop compared to 69% in the biofilm loop, indicating stronger adhesion in the presence of biofilms. Subsequent flushes mobilized more material from the biofilm experiment, particularly under higher shear stress. Microscopy revealed that biofilms captured both fine and large particles (up to 30 μm), and even with limited surface coverage (~3%), substantially enhanced particle adhesion. While the biofilms developed under experimental conditions may differ from mature biofilms in actual DWDSs, the results demonstrate that biofilms have the potential to promote particle accumulation and resist their mobilization under high-shear events. Despite the ubiquity of biofilms in DWDS, these results may help water utilities improve pipe cleaning strategies and better manage material accumulation within the systems.

Water impact

Drinking water discolouration is caused by the release of biofilm and particulate materials that accumulate inside pipe networks. This study investigates the role of biofilms in facilitating the capture of iron oxide particles suspended in the flow and enhancing their adherence to the pipe wall, thereby increasing the resistance of accumulated materials to mobilization. These findings will support water utilities in improving pipe cleaning strategies and reducing discolouration risks in operational networks.

Introduction

Drinking water distribution systems (DWDS) are typically designed to operate over several decades. As these systems age, metallic components corrode, biofilms develop, and materials progressively accumulate on the inner walls of pipes.[1,2] The accumulation of such deposits has long been recognized in DWDSs, particularly due to the early, widespread use of unlined cast iron pipes, which frequently caused "red water" events triggered by the resuspension of iron corrosion scales.[3,4]

In recent decades, new concerns have emerged regarding material accumulation in modern plastic pipes.[5–7] Studies have detected a broad spectrum of contaminants within these deposits, including contaminants of emerging concern (CECs), toxic heavy metals (*e.g.*, arsenic, lead), pathogenic microorganisms, and antimicrobial resistance genes (ARGs).[8–15] This growing body of evidence is prompting water utilities to implement pipe-cleaning programs to safeguard drinking water quality. Pipe flushing emerged as the primary tool to assess and mitigate material accumulation. However, flushing can only account for mobile fractions of pipe wall material, and it remains limited due to the vast physical scale and the limited accessibility of underground pipes that make up DWDSs. As an alternative, researchers are striving to better understand the mechanisms underlying material build-up, supporting the development of predictive models and more effective strategies for maintaining clean pipes.[1,16–18]

Department of Civil Engineering, Queen's University, Kingston, Ontario, Canada. E-mail: asb9@queensu.ca, yves.filion@queensu.ca, ben.anderson@queensu.ca

A widely-referenced model that significantly advanced the understanding of water discolouration is the variable condition discolouration model (VCDM), developed from its predecessor, PODDS.[17,19] VCDM predicts increases in water turbidity in response to changes in pipe flow conditions. VCDM uses the wall shear stress (WSS) to determine whether materials on the pipe wall are in a state of accumulation or detachment. To do this, it compares WSS to the material shear strength (MSS) — the force that binds materials to the pipe wall. The model estimates the "load of material" (*i.e.*, discolouration potential) in a pipe section using a material function with coefficients representing accumulation and detachment dynamics. A key feature of VCDM is its representation of discolouration potential as a sum of multiple material layers, each with a distinct MSS. Notably, layers with lower MSS contribute more significantly to turbidity upon detachment (*e.g.*, in DWDS dead ends), while layers of different MSS accumulate at varying rates and eventually reach a saturation point in terms of discolouration potential.[17,20]

The performance of the VCDM has been validated through multiple studies and has been applied in proactive maintenance strategies to reduce discolouration risk.[6,16,20–22] However, its empirical nature requires calibration for each application, limiting broader implementation. Furthermore, the model exclusively outputs turbidity, which reflects suspended solids concentration (SSC) *via* light scattering. As such, the VCDM and similar turbidity-based models can only estimate material loads indirectly. They cannot identify specific material types (*e.g.*, biofilms, iron oxide particles) or account for materials that remain attached under maximum flow conditions (*i.e.*, where MSS > maximum WSS). Additionally, the relationship between turbidity and SSC is often complex due to variability in particle size and composition, leading to potential inaccuracies when modelling material accumulation and detachment solely through turbidity data.[23–26]

To address these limitations, researchers have focused on linking discolouration mechanisms to the specific materials that accumulate in DWDSs. Two primary contributors have been identified: (1) iron oxide particles, and (2) biofilms.[1,27,28]

Iron oxide particles are abundant in systems with corroded pipes but are also found in plastic pipes and even in networks with no metallic components.[22,29,30] It is hypothesized that these particles originate from upstream corrosion hotspots (*e.g.*, old cast iron mains, valves) and are transported downstream and deposited along the pipe network.[31] Alternatively, dissolved iron, which is commonly present in drinking water and sometimes at elevated concentrations due to the release of iron-based coagulant residuals in the water treatment process, may precipitate under certain chemical conditions (*e.g.*, pH or temperature changes) or bind with organic matter at the pipe wall.

Recent experiments examining the attachment of suspended iron oxide particles to clean polyvinyl chloride (PVC) pipes have shown that attachment is primarily governed by SSC, with flow velocity and WSS having limited influence under typical operational conditions.[23] Surprisingly, particles as small as 1 μm were able to loosely settle at the pipe invert, contrary to expectations from sediment theory under turbulent flow.[32] Moreover, a secondary mechanism involving the anchoring of particles in the surface roughness of PVC pipes produced a range of MSS values,[23,33] consistent with VCDM predictions. This highlights pipe wall roughness as a critical factor that influences material accumulation.

Conversely, biofilms, present in all DWDSs, are believed to account for a large portion of organic matter observed during pipe flushing.[34–37] Although biofilms themselves are generally translucent and contribute little to turbidity,[38] their characteristics align closely with the material layer dynamics modelled in VCDM. For instance, biofilms exhibit cohesive forces that may explain the formation of layered deposits and varying MSS.[7] Active biofilm cells are typically concentrated in deeper layers that are not readily detached, allowing regrowth post-flushing.[39] Biofilms also produce extracellular polymeric substances (EPS) that aid in nutrient capture and promote the fixation of dissolved materials.[40–42] The adhesive properties of EPS may also facilitate the entrapment of suspended particles, reinforcing biofilm growth and material accumulation.

In summary, there is strong evidence that both iron oxide particles and biofilms contribute to material accumulation and water discolouration in DWDSs. Existing models, however, are limited to indirect quantification of accumulated material based on turbidity. They are unable to differentiate between specific contributors to discolouration or to account for potential synergistic effects between particles and biofilms. Addressing these limitations will be essential for developing more accurate models and effective management strategies for maintaining drinking water quality.

Given these research gaps, the aim of this paper is to investigate how biofilms contribute to the accumulation and mobilization of particulate material in PVC pipes. The specific objectives are to:

1. Quantify the contribution of biofilms to the attachment of suspended iron oxide particles to the pipe wall of PVC pipes relative to the no-biofilm case;

2. Quantify effect of biofilms on the mobilization of pipe wall particles provoked by a flow rate increase in both the forward and reverse directions relative to the no-biofilm case; and

3. Characterize both biofilms and particles attached to the pipe wall of PVC pipes before and after their attachment and mobilization using microscopy imaging.

To achieve these objectives, a unique set of experiments was conducted in a pilot-scale laboratory, employing

innovative methods to quantify and characterize both biofilms and particles within the pipes.

Methods

Overview of experiments

Experiments were conducted in the Drinking Water Distribution Laboratory (DWDL) at Queen's University, using a full-scale pipe loop pilot built with IPEX Blue Brute PVC pipes, with an internal pipe diameter of 108 mm (4″) and a length of ~200 m. The system was designed to mimic hydraulic conditions of operational DWDSs to investigate drinking water quality deterioration during its transport in pipe networks. The pipe loop can be operated either by recirculating water between pipes and a 3.5 m^3 tank (closed configuration), or without recirculation, by discarding it entirely at a drain at the end of the pipes (open configuration) – Fig. 1. In the open configuration, the water tank is continuously replenished with local drinking water from Kingston – ON. This drinking water is filtered with a common household particle filter (melt-blown 1 micron) to avoid introducing external materials into the pipes. A set of valves allows the operation of the pipe loop in both flow directions (forward and reverse). In addition, the entire laboratory is situated in a temperature-controlled chamber, which was maintained at 16 °C for these experiments.

Two identical experiments were conducted using the same pipe loop with different initial pipe conditions: 1) biofilm are present, and 2) no-biofilms. For the biofilm experiment, the pipe walls of the pipe loop were pre-conditioned with biofilms for 28 days (see biofilm pre-conditioning and growth section below). In contrast, the no-biofilm experiment began with disinfected and clean pipe walls, which were exposed to free chlorine concentrations above 20 mg L^{-1} for 24 h and flushed at a high flow rate of 15 L s^{-1} using the open configuration.

From the pipe loop initial condition, two experimental phases were used in this investigation, both employing the open configuration of the pipe loop: 1) a particle attachment phase, and 2) a particle mobilization phase. The hydraulic and water quality conditions of the pipe loop during the experiments are presented in Tables 1 and 2, respectively.

In the particle attachment phase, a controlled injection of suspended particles was performed at the midpoint location of the pipes (Fig. 1) to promote their attachment to the pipe wall under steady-state conditions. The mobilization phase employed different flushing strategies to mobilize particles from the pipe wall. Both phases were carefully replicated for both experiments, isolating the presence or absence of biofilm on the pipe wall as their only difference. Full details of each experimental phase and assessment methods are described in their respective sections below.

Biofilm pre-conditioning and growth

The pre-conditioning of the pipe walls with biofilms was exclusive to the biofilm experiment. For this, the pipe loop was operated at a steady-state flow of 0.6 L s^{-1} and water pressure of 280 kPa, in a closed configuration, for a period of 28 days to allow biofilm growth under conditions that partially mimic operational DWDSs. To accelerate the slow development of biofilms in new drinking water pipe sections,

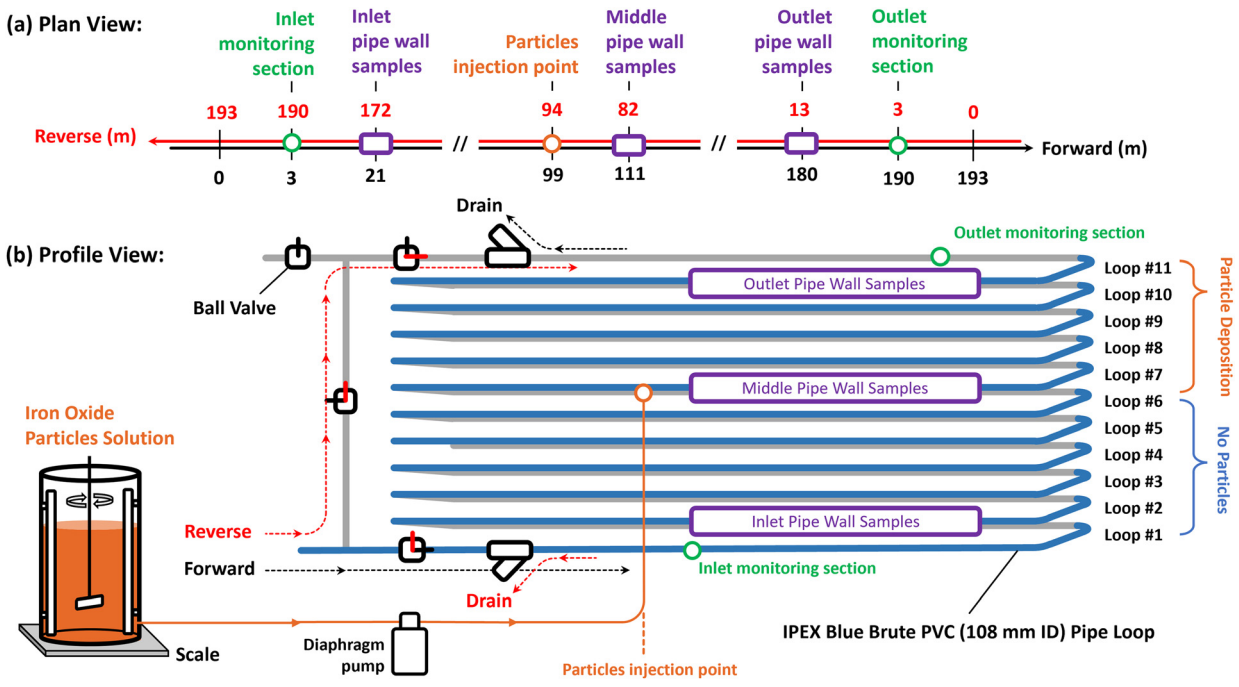

Fig. 1 Pipe loop schematic highlighting the i) particles injection point; ii) pipe wall sampling positions; iii) flow path in the forward and reverse directions; iv) monitoring sections; vi) upper pipe loop half where particles were deposited; and vi) lower pipe loop half free of deposited particles.

Table 1 Hydraulic conditions of the pipe loop during experiments

Exp. stage	Flow direction	Flow (L s^{-1})	Velocity (m s^{-1})	Re[a]	WSS[b] (Pa)	HRT[c] (min)
Biofilm grow & particles injection	Forward	0.6	0.07	7000	0.02	50.9
Flush step F1	Forward	6.5	0.71	76 600	1.20	4.7
Flush step F2	Reverse					
Flush step F3	Forward	11.0	1.20	129 700	3.09	2.8
Flush step F4	Reverse					

[a] Reynolds number. [b] Wall shear stress. [c] Pipe loop hydraulic retention time.

the water in the pipe loop was initially inoculated with 2 L of a concentrated solution of microorganisms sourced from local tap water.

Microorganisms were captured in granular activated charcoal filter columns (GACs) that were continuously operated for more than a year. In this system, local tap water was maintained at 20 °C. The first GAC column stripped background disinfectants (the column was renewed when disinfectants were detected in the effluent), and the second GAC column provided a surface for drinking water microorganisms to attach and develop biofilms. Upon biofilm maturation, a stable output of microorganisms was detected in the GAC filter effluent, commonly released from biofilms to colonize new surfaces. To produce the final concentrated microorganism solution, the GAC effluent was combined at 1 : 1 ratio with Nutrient Broth No. 3 (Millipore Sigma) and incubated under agitation at 20 °C for one week. This nutrient solution was selected for its non-specific microorganism growth potential, aiming to support the proliferation of diverse microbial communities.

Before introducing the microorganism solution into the pipe loop, the pipes were disinfected and cleaned as previously described. The fresh, filtered drinking water in the system was dechlorinated with sodium thiosulfate, and no disinfectants were used during the pre-conditioning period. Starting on day 0, 3 L of Nutrient Broth No. 3 (Millipore Sigma) with a concentration of 13 g L^{-1} was added weekly to support biofilm development. The system volume remained constant throughout the growth period, apart from nutrient additions and small-volume sample collections. The closed system configuration facilitated organic mass balance calculations for assessing biofilm development. During the entire growth period, water pH remained stable at around 8.1, and dissolved oxygen remained saturated at ~12 mg L^{-1} (0.2 μm filtered air was constantly supplied to the tank through a large aquarium aerator).

Table 2 Water quality conditions of the pipe loop during experiments

Water quality parameter	Value
pH	8.15
Water temperature (°C)	16.7
Dissolved oxygen (mg L^{-1})	11.0–13.2
Specific conductivity (μS cm^{-1})	335
Turbidity (NTU)	0.1–1.0

These values indicate no substantial changes in water chemistry (Table 2) occurred during the growth period, apart from the fixation of dissolved constituents as microbial organic mass.

Bulk water from the system was sampled weekly and tested for: 1) suspended solids concentration (SSC), volatile suspended solids concentration (SSCv), and fixed suspended solids concentration (SSCf); 2) total dissolved solids (TS), volatile total dissolved solids (TSv), and fixed total dissolved solids (TSf); 3) adenosine triphosphate concentration (ATP); and 4) total cell counts *via* flow cytometer (FC). Pipe wall samples were also collected weekly from multiple locations and tested for surface cell density using FC and imaged with a fluorescence microscope using SYTO9, a DNA-label dye (see microscopy imaging of pipe wall samples).

In summary, data collected during the biofilm growth period indicate that microorganisms rapidly established stable populations in both bulk water and on pipe walls, progressively consuming dissolved nutrients and fixing them as organic matter. The TSv of the bulk water was initially measured at ~470 mg L^{-1} but was completely depleted by ~20 days. At that point, a sharp drop in microorganism cell counts was observed in the bulk water (Fig. S1), suggesting that biofilms consumed all available nutrients (including planktonic cells) and entered in starvation. Suspended solids concentrations (SSC) from this period were 100% volatile and increased gradually over 28 days, peaking at 1.7 mg L^{-1} on day 22 before dropping to 0.6 mg L^{-1} during the final week. This supports a shift in biofilm activity around day 20 and aligns with the expected behavior that the SSCv will increase with a nutrient abundance and particle release, followed by nutrient harvesting during starvation.[40]

Additional details about the biofilms at the end of the pre-conditioning step are presented in the results section. This overview was kept brief, as biofilm development is not the focus of this manuscript. The complete dataset for this period is available in the SI file (Fig. S1–S4). Experimental limitations of the biofilm growth method are discussed in the experimental limitations section.

Particle attachment phase

During the particle attachment phase, a concentrated solution of ferric iron (Fe_2O_3) was injected at the midpoint of the pipe loop (Fig. 1) under steady-state flow conditions (Table 1).[23] A 400 L mixing tank kept the particles suspended,

and a diaphragm pump drew the solution from the bottom of the tank and pumped it into the loop at the centerline of the pipe cross-section at the midpoint location. The particles quickly mixed with the turbulent flow, forming a suspended particle plug that traveled downstream. The plug was discarded at the loop outlet. The plug length (240 m) was defined by the product of the fluid velocity (Table 1) and the ~1 h injection period. After injection, the pipe loop flow rate was maintained for ~40 minutes to flush 1.5× the volume of half the pipe loop length (~95 m). This ensured that all suspended particles exited the pipe loop before the pumps were stopped and prevented particle attachment under stagnant conditions.

Ferric iron particles were selected due to their relevance to pipe corrosion and water discoloration, as well as their high chemical stability and insolubility. A target concentration of 5 mg L^{-1} was used based on data of previous experiments that achieved turbidity readings of ~30 NTU.[23] This turbidity level is common during discolouration events in DWDS.[22] Prior to use, particles were divided into packages of equal mass and particle size using a rotary splitter, ensuring consistency across experiments. The solution was mixed for at least 10 minutes before and throughout the injection. Multiple samples of the solution were collected at the diaphragm pump inlet and tested for SSC using gravimetric analysis.[43] SSCv and SSCf were also determined by combusting fiberglass filters at 450 °C. The total mass of suspended solids injected into the pipes was calculated by multiplying the average SSC by the precise injected volume (measured with a large industrial scale).

SSC, SSCv, and SSCf of the particle plug in the pipes were assessed *via* three samples collected at the outlet, timed at 25%, 50%, and 75% of the plug length. Online turbidimeters (Hach TU5300sc) were used to continuously monitor turbidity at both the inlet and outlet (1 Hz resolution). Small pumps were used to draw water from the center of the pipe cross section to ensure consistent flow through the turbidimeter under varying pressure conditions.

The flux of suspended sediments (FSS) through the pipe loop outlet was calculated using eqn (1). Turbidity values were converted to SSC values by means of calibration coefficients (α) which were calculated by regressing turbidity against SSC measured in the bulk water samples. Integrating the FSS over the particle injection period yielded the total mass of suspended particles that exited the system. The accumulated mass in the loop was determined by subtracting this from the injected mass. The organic/inorganic fractions were estimated similarly.

$$FSS = \alpha \times Turb \times Q \quad (1)$$

Equation 1: FSS (mg s^{-1}) is the flux of suspended sediments, Turb is the water turbidity, α (mg L^{-1} NTU^{-1}) is the turbidity-to-SSC conversion coefficient, and Q (L s^{-1}) is the flow rate.

Particle mobilization phase

In the mobilization stage, four flushing steps (F1–F4) were used to mobilize particles and biofilms from the pipe walls and evaluate their behavior under mechanical stress. The first two steps (F1 and F2) were conducted at 6.5 L s^{-1} in the forward direction (F1) and in the reverse direction (F2). Flushing step F3 was performed in the forward direction and flushing step F4 in the reverse direction; both were performed at a higher flow rate of 11.0 L s^{-1} (Table 1). This strategy tested the resistance of adhered materials to flow direction[44] and magnitude.[33] All flushing steps used the open configuration and followed this sequence:

1. Flow rate ramp-up from 0 L s^{-1} to target;
2. Maintain the flow rate of 2.5× pipe volumes;
3. Flow rate ramp-down to 0 L s^{-1}.

For each flushing step, a composite water sample was collected at the outlet (inlet for F2 and F4), during the period corresponding to 25–75% of the first pipe volume. The sampling strategy varied depending on expected detachment locations:

- F1 and F2: assumed detachment from the upper half of the pipe loop exposed to the particle plug (Fig. 1).

- F3 and F4: assumed detachment from the entire loop due to possible particles reattachment during F2 (reverse flush).

All samples were tested for SSC, SSCv, and SSCf. Turbidity was continuously monitored as in the particle attachment phase.

For reverse flows (F2 and F4), turbidimeter intake probe orientations were reversed to maintain consistent conditions. FSS was again calculated using eqn (1) and α values that were specific to each flushing step. However, turbidity changes were smaller (especially for F2–F4), so FSS was corrected to remove background turbidity that was not caused by particle detachment from the pipes. Detached particle contribution was assumed only during the initial passage of 2.5 pipe volumes. Total mass mobilized was then calculated by integrating FSS over each flushing step.

Microscopy imaging of pipe wall samples

Pipe wall conditions were analyzed by collecting dedicated pipe wall samples for microscopy imaging. The DWDL sampling system uses cut-out sections of PVC pipes that make up the pipe loop, mounted with 3D-printed supports.[45] This is done to align the sample surface with the pipe wall (~0.1 mm), and to ensure that the pipe coupon is exposed to the same flow conditions as the rest of the pipe. Pipe coupon sampling locations included three longitudinal positions: 1) inlet (~23 m), 2) midpoint (~113 m), 3) outlet (~185 m), and three circumferential positions: 1) invert, 2) springline, 3) obvert.[45]

For these experiments, samples were taken from the invert at all longitudinal positions (IN-INV, MID-INV, OUT-INV) and the obvert at the midpoint location (MID-OBV). Samples were collected before and after particle injection,

and after F1 flushing. Samples were gently rinsed with 40 mL of DI water poured over a 45°-inclined sample surface to remove loose material. No-biofilm experiment samples were stored at 4 °C. Biofilm experiment samples were fixed with 5% glutaraldehyde for 15 minutes, rinsed three times with DI before storage in similar conditions. Prior imaging, biofilm experiment samples were individually stained with SYTO9 (ThermoFisher) at a concentration of 20 μM for 15 minutes, followed by three 1 minute deionized water (DI) rinses.[46]

Prepared samples were mounted in microscopy dishes under DI water and imaged using a fully automated Nikon Ni-E epi-fluorescence microscope with water immersion lenses at 100× and 400× magnifications. Water immersion was used to preserve biofilms hydration and enhance image quality with a higher numerical aperture. No-biofilm experiment samples were imaged in brightfield mode only. Biofilm experiment samples were imaged in both brightfield and fluorescence modes (FITC/GFP cube). Light settings were standardized across all samples.

Microscope automation captured 18 FOVs at 100× and 5–30 FOVs at 400×, centered on the sample. For biofilm experiment samples, only 5 FOVs were captured at 400× due to longer acquisition times. A *z*-stack captured the full vertical focus range, which then collapsed into a single focused image per FOV using the proprietary *z*-stacking feature in the Ni-Elements microscope software.

Brightfield images were taken in color (RGB), while fluorescence images were captured in grayscale (light intensity-based) but displayed in green for easier visualization. All images were captured at a resolution of 2880 × 2048 pixels, with each pixel corresponding to 0.43 μm at 100× and 0.11 μm at 400× magnification.

Images were processed using algorithms written in Python to create mosaics and overlay the fluorescence images on the brightfield images. This enabled clear visualization of both biofilms and iron oxide particles on the pipe wall surface.

Results

Quantification of particles attached to pipe walls

Results from the particle attachment phase for the biofilm and no-biofilm experiments are presented in Table 3. During the passage of the particle plugs through the pipe loops, the suspended sediment concentration (SSC) averaged 4.5 mg L^{-1} and was slightly higher in the biofilm experiment. The turbidity of the plugs remained stable during their passage through the pipes (Fig. S5); however, a minor change in the operational flow rate of the turbidimeters caused a large difference in the average turbidity between the experiments (Table 3, Fig. S5). The consistency of SSC measurements and the identical setup of the experiments indicate that the turbidimeter flow rate was the sole factor responsible for this discrepancy in plug turbidity. Furthermore, mass estimations based on turbidity data remained consistent due to the appropriate calibration of the turbidity-to-SSC coefficients for each experiment (Table 3).

By the end of the particle attachment phase, a total mass of 26.8 g and 23.3 g was estimated to have accumulated in the upper half of the pipe loop downstream the particle injection position (Fig. 1) for the biofilm and no-biofilm experiments, respectively (Table 3). This indicates that 66% of the total mass of injected particles attached to the pipe walls in the no-biofilm experiment. The presence of biofilms facilitated the attachment of an additional 6% of suspended particles, resulting in a total attachment of 72% in the biofilm experiment.

In addition, the original concentrated solution of iron oxide particles had 98% inorganic SSC, while samples from the particle plugs indicated a reduction of inorganic SSC to 95% (Table 3). This shift suggests that a higher proportion of the inorganic mass of suspended particles was attached to

Table 3 Results from the particle attachment phase of the experiments

Stage	Variable	Biofilm	No-biofilm
Concentrated solution of Fe_2O_3 particles injected in the midpoint location of the pipe loop	SSC[a] [mg L^{-1}]	182.4	173.4
	Injected volume [L]	204.6	202.9
	Injected mass [g]	**37.32**	**35.18**
	Organic fraction[b] [g]	0.60 (2%)	0.57 (2%)
	Inorganic fraction[c] [g]	36.71 (98%)	34.61 (98%)
Plug of suspended particles at the outlet location of the pipe loop	SSC[a] [mg L^{-1}]	5.22	4.87
	Turbidity [NTU]	34.5	22.2
	Approximate plug volume [L]	2160	2160
	α[d] [mg L^{-1} NTU^{-1}]	0.151	0.219
	Exited mass [g]	**10.51**	**11.85**
	Organic fraction[b] [g]	0.54 (5%)	0.61 (5%)
	Inorganic fraction[c] [g]	9.97 (95%)	11.24 (95%)
Mass balance calculations: accumulated = injected – exited	**Accumulated mass [g]**	**26.81 (72%)**	**23.31 (66%)**
	Organic fraction [g]	0.07 (0%)	−0.04 (0%)
	Inorganic fraction [g]	26.74 (100%)	23.37 (100%)

[a] Suspended sediment concentration measured from triplicate samples. [b] Calculated based on the volatile fraction of SSC. [c] Calculated based on the fixed fraction of SSC. [d] Turbidity-to-SSC coefficient calibrated using SSC measurements.

the pipes, compared to their smaller organic fractions, which remained in suspension. The difference between the total organic mass entering and exiting the pipe loops remained within 0.2% of the total injected mass. This suggests that the particles accumulated on the pipes were predominantly inorganic.

Dynamics of particle mobilization during flushing

Fig. 2 shows the flux of suspended sediments (FSS) at the outlet location of the pipe loop (Fig. 1) for the four sequential flushing steps conducted after the particle attachment phase, in both the biofilm and no-biofilm experiments. Note that for flushing steps F2 and F4, the outlet location corresponds to the inlet of the previous experimental stages due to flow direction reversal (Fig. 1). The important difference in the graph scales is highlighted, reflecting the disproportionately larger amount of particle mobilization expected during the first flushing step (F1; Fig. 2a).

Vertical dashed lines in Fig. 2 denote the turnover of the pipe loop water volume during each flushing step. These volume turnover values approximately indicate the longitudinal position where particles detached from the pipe wall, which is expected to rapidly occur during the pump flow ramp-up (approximately 30 seconds[47]). Thus, the profiles in Fig. 2 highlight the pipe loop locations that contributed to the highest material mobilization.

In both experiments, F1 (Fig. 2a) mobilized the greatest mass of accumulated materials (organic and inorganic), showing distinct peaks shortly after 0.5 volume turnovers. These findings align with previous studies,[23,31,44] as the FSS peaks correspond to the midpoint of the pipe loop where particles were introduced during the particle attachment phase. The rapid settling of large particles near their injection point resulted in substantial local accumulation, producing the pronounced FSS peaks observed in F1. There is also a noticeable difference between the pre-peak FSS profiles for the biofilm and no-biofilm experiments (F1; Fig. 2a). The no-biofilm experiment profile shows a steady increase in particle mobilization between 0 s and 120 s (prior to the start of the peak), suggesting that after initial accumulation near the injection point, particle attachment rapidly decreased along the pipe length toward the outlet. In contrast, the FSS profile in the biofilm experiment shows a sharp rise in FSS up to 60 s (due to flow ramp-up), followed by a stable FSS of around 40 mg s^{-1} until the start of the peak at 120 s. This suggests a more uniform and substantial attachment of particles along the pipe in the presence of biofilms, likely enhanced by EPS in the biofilm. This stability of FSS can be caused by the detachment of consistent biofilm EPS layers with similar proportions of iron oxide particles. This suggests that biofilm EPS collected a similar quantity of particles along the pipe loop length. Previous studies support the hypothesis that EPS plays an important role in capturing particles through adhesion-related processes.[53]

Additionally, the slight increase observed in the FSS profile for the biofilm experiment between 220 s and 290 s (F1; Fig. 2a) indicates material detachment from upstream regions of the pipe loop, upstream of the particle injection point (Fig. 1). This suggests that the detachment of EPS layers from biofilms may have also contributed to FSS in this region. Notably, the FSS profile of flushing step F1 in the

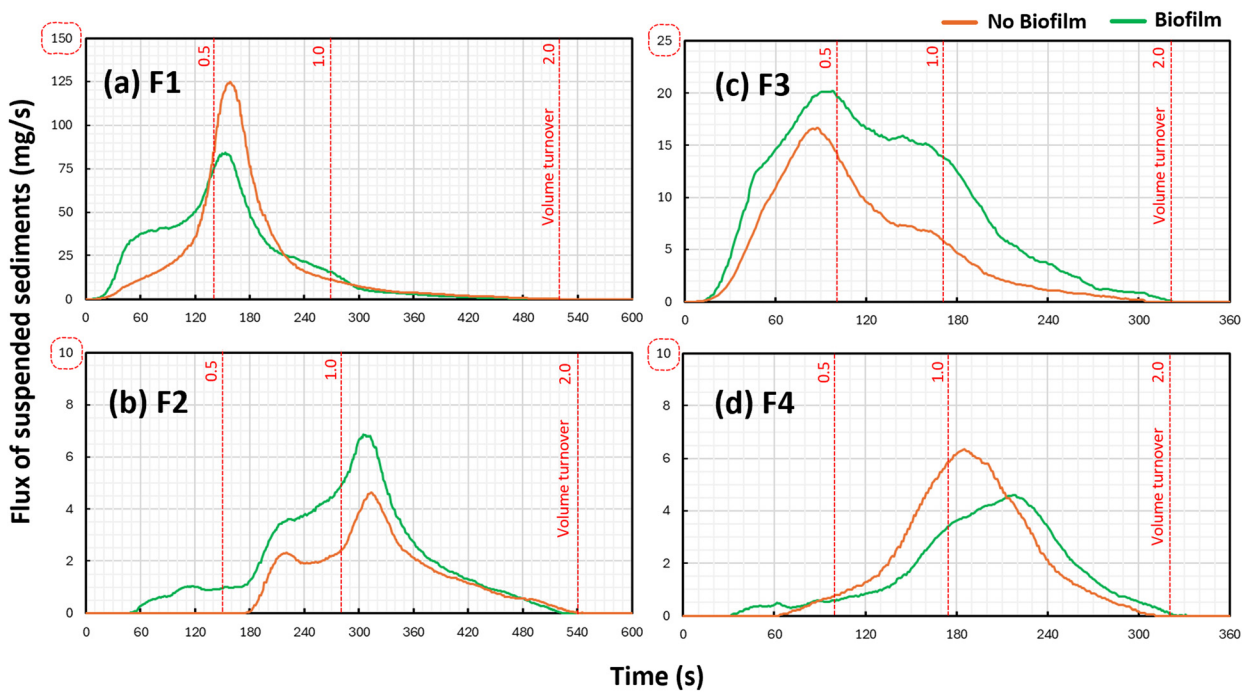

Fig. 2 Flux of suspended sediments (FSS) profiles during the flushing steps F1–F4 of both biofilm and no-biofilm experiments. Vertical dashed lines correspond to the pipe loop volume turnover during each flushing step.

biofilm experiment resembles turbidity patterns commonly reported in discoloration literature, where accumulated materials possess some adhesion strength with the pipe walls.[22]

In the second flushing step (F2; Fig. 2b), where flow direction was reversed but flow rate remained the same as in F1, FSS values were substantially lower for both experiments. The similarity in FSS profiles suggests that particles mobilized in F2 after resisting the shear forces during F1 were attached to the pipe wall through similar mechanisms. The mobilization of these particles during F2 also indicates a flow-direction-dependent resistance. In the no-biofilm experiment, no particles were mobilized from the lower half of the pipe loop (up to 180 s; Fig. 2b), while in the biofilm experiment biofilms attached to the pipe wall in the first half of the pipe loop were mobilized between 60 and 180 s. The mobilization of biofilms caused a slight positive offset (~1 mg s^{-1}) of the F2 FSS compared to the no-biofilm experiment.

The smaller peaks of the FSS profiles of F2 (~220 s; Fig. 2b) correspond to the particle injection point, while the higher peaks after one volume turnover (~310 s; Fig. 2b) indicate that particles accumulated in the wye fitting and closed ball valve located at the outlet section of the pipe loop during the particle attachment phase and flushing step F1.

When the flow was reversed, trapped particles in the wye at the outlet were exposed to high shear stress and mobilized to the inlet.[44]

The third flushing step (F3; Fig. 2c) was performed in the forward flow direction but at a higher flow rate (11 L s^{-1}). Here material mobilization increased compared to F2, but remained lower than F1. This result aligns with previous findings that indicate that higher wall shear stress mobilizes more strongly adhered materials.[31,48,49] The FSS profiles of the biofilm and no-biofilm experiments again show strong similarity and both peak at the particle injection point. However, between 120 s and 170 s of Fig. 2c, both profiles exhibit a plateau before completing 1.0 volume turnovers. This suggests a material mobilization from the first half of the pipe loop that was especially pronounced in the biofilm experiment. Since no material was mobilized from this pipe region in F1 or F2 for the no-biofilm experiment, this mobilization at F3 suggests a possible reattachment of particles to the pipes during F2 (reverse flush). The higher FSS in the biofilm experiment during F3 (Fig. 2c) also suggests greater reattachment, potentially facilitated by residual biofilm EPS that resisted mobilization during F1 and F2.

Finally, in the fourth flushing step (F4; Fig. 2d), conducted at the same flow rate as F3 but in the reverse direction, a small amount of material was mobilized in both experiments. The FSS profiles are nearly identical, differing only slightly in magnitude and peak location. The main peaks again reflect mobilization of trapped material in the wye dead-end section at the outlet. Contributions from the actual pipe loop are very small (approximately 0.5 mg s^{-1}), indicating that the directional resistance of the biofilm and the particles seen between F1 and F2 was greatly reduced at the higher flow rate.

Quantification of particle mobilization during flushing

The final load of material mobilized from the pipe loop during each flushing step for both experiments is shown in Table 4. A total mass of 13.20 g and 15.09 g were mobilized from the pipe loop for the no-biofilm and biofilm experiments, respectively. These numbers corresponded only to ~56.5% of the material accumulated loads for both experiments and highlight a substantial imbalance of the particles entering and leaving the pipes during these experiments. It is important to highlight that such discrepancy is unlikely to be caused by particle resistance to mobilization since flushing flow rates as high as 11 L s^{-1} (3.1 Pa) are known to mobilize almost all material accumulated on pipes.[23,31] They might be explained, however, by inaccuracies of the turbidity-to-SSC conversion coefficients that are likely unstable during the first flushing step due to a high variation of particle size distribution mobilized from different locations of the pipe loop.

The largest fractions of mobilized material occurred in the first flushing step – F1 and corresponded to 71% and 78% of the total material mobilized in the biofilm and no-biofilm experiments, respectively. The mobilization of an extra 7% of materials in the F1 flushing step in the no-biofilm experiment highlights the lower adhesion forces of particles to the pipe walls, which is also confirmed by the sharp peak of F1 in Fig. 2a. This suggests that biofilms not only increased the attachment of particles by 6% but also increased their mobilization resistance at an even higher rate of 7%.

The particles with higher resistance to mobilization are found in the subsequent flushing steps F2, F3 and F4. The F2 and F4 flushing steps mobilized an average of 5% of the total material mobilized across all flushing steps in the biofilm and no-biofilm experiments (Table 4). It is worth noticing that in these flushing steps, where flow direction was reversed, there was a significant material load contribution from the wye dead-end at the outlet of the pipe loop as explained in the previous section. Meanwhile the second largest differences were identified in the F3 flushing step, where the fraction of the total material mobilized corresponded to 19% and 12% in the biofilm and no-biofilm experiments, respectively. The increase of wall shear stress during the F3 step likely promoted the mobilization of biofilm layers with adhered particles, leading to an additional 7% of material mobilization in the biofilm experiment.

In terms of organic solids, SSC samples collected from flushing steps revealed that approximate fractions of 16% and 12% of the total mobilized mass were organic in the biofilm and no-biofilm experiments, respectively (Table 4). Most of organic matter obtained from the biofilm experiment is expected to be biofilm EPS. In comparison, it is unclear

Table 4 Results from the flushing stage of the experiments

	Biofilm					No-biofilm				
Flushing stage	F1	F2	F3	F4	Total	F1	F2	F3	F4	Total
Mobilized turbidity [NTU L]	8266	494	896	226	**9883**	3157	134	372	138	**3801**
α^a [mg L^{-1} NTU^{-1}]	1.327	1.774	3.644	3.545		3.437	4.704	4.585	4.466	
Mobilized mass [g]	**10.67 (71%)**	**1.03 (7%)**	**2.88 (19%)**	**0.51 (3%)**	**15.09 (100%)**	**10.36 (78%)**	**0.61 (5%)**	**1.64 (12%)**	**0.59 (4%)**	**13.20 (100%)**
Organic fraction^b [g]	1.46 (10%)	0.19 (1%)	0.69 (5%)	0.15 (1%)	**2.49 (16%)**	0.98 (7%)	0.16 (1%)	0.22 (2%)	0.23 (2%)	**1.59 (12%)**
Inorganic fraction^c [g]	8.21 (61%)	0.84 (6%)	2.19 (15%)	0.36 (2%)	**12.60 (84%)**	9.38 (71%)	0.45 (3%)	1.43 (11%)	0.36 (3%)	**11.61 (88%)**
Mobilized/accumulated					**56.3%**					**56.6%**

^{a} Turbidity-to-SSC coefficient calibrated using SSC measurements. ^{b} Calculated based on the volatile fraction of SSC. ^{c} Calculated based on the fixed fraction of SSC.

what the origin of the organic mass was for the no-biofilm experiment, since the pipes were disinfected and flushed at elevated flow rates prior to the experiment, and no suspended solids were detected in the tap water. It is hypothesized that iron oxide particles might have absorbed small amounts of organic matter dissolved in the water, thereby adding organic fractions to the suspended solids of the flushing samples. Meanwhile, slightly higher organic fractions of mobilized mass occurred in the biofilm experiment for the flushing steps F1 and F3 (Table 4), which suggests that larger quantities of biofilms were mobilized in these flushing steps. However, the presence of biofilms alone was not sufficient to explain the differences in the organic fraction of mobilized mass in the F3 flushing between the biofilm and no-biofilm experiments.

In comparison, considering just the inorganic fractions in the flushing step F3 (Table 4), the mobilization fraction of 15% in the biofilm experiment is still higher than the 11% mobilization fraction in the no-biofilm experiment. This suggests that iron oxide particles accumulated on the biofilms in the biofilm experiment, and that they possessed a higher overall resistance to mobilization from previous flushing steps F1 and F2.

Characterization of particles and biofilms on pipe walls with microscopy

A large set of microscopy images was collected from pipe wall samples in both the biofilm and no-biofilm experiments to characterize the attachment of particles and biofilms on the pipe surface. The figures included in this section represent a subset of the full dataset, which is available in a data repository as SI of the manuscript. Microscopy images from the no-biofilm experiment were captured only using brightfield microscopy. In contrast, images from the biofilm experiment consist of fluorescent images highlighting DNA-stained biofilms using SYTO9 overlayed onto brightfield images. Microorganism cells within the biofilm have a higher concentration of DNA and therefore produce a higher light intensity of fluorescent images stained with SYTO9. Biofilm EPS structures were also partially visible in the images due to the presence of extracellular DNA.

In both experiments, no consistent attachment of particles or biofilms was observed on samples collected from the obvert (top) position of the pipe wall. Therefore, only samples from the invert (bottom) positions across the three longitudinal pipe loop locations (inlet, midpoint and outlet) were analyzed. Previous research suggests that particle attachment at the obvert is limited in the absence of any biofilms.[23] However, the lack of uniform biofilm growth around the pipe circumference remains unclear and is discussed further in the experimental limitations section.

A key consideration in interpreting the microscopy images from the no-biofilm experiment is that some samples initially showed visible loose particles on their surface upon extraction, which were also found on bulk water samples from the flushing step F1 (Fig. S6). These particles were removed during the sample washing step, which employed a gentle stream of deionized (DI) water. Consequently, these loosely attached particles are not present in the final microscopy images.

Pipe wall conditions prior to particle addition. Fig. 3 presents microscopy images of pipe wall samples collected before particle addition in both the no-biofilm and biofilm experiments. Samples were obtained from the invert pipe position at the inlet, midpoint, and outlet of the pipe loop and imaged at 100× (Fig. 3a–f) and 400× (Fig. 3g–l) magnifications.

In the no-biofilm experiment, all pre-particle samples were free of both particles and biofilms (Fig. 3a–c and g–i). In contrast, samples from the biofilm experiment showed consistent biofilm cluster formation at all three pipe locations (Fig. 3d–f). These clusters were highly heterogenic, covered approximately 3% of the surface area (observed exclusively with DNA stain) and appeared isolated. This is typical biofilm behavior in the early stages of biofilm growth.[42,54] Higher magnification images (Fig. 3j–l) revealed diverse biofilm morphologies, including bridge-like structures connecting clusters (Fig. 3l), likely indicative of an early-stage, multi-species biofilm. Multiple individual

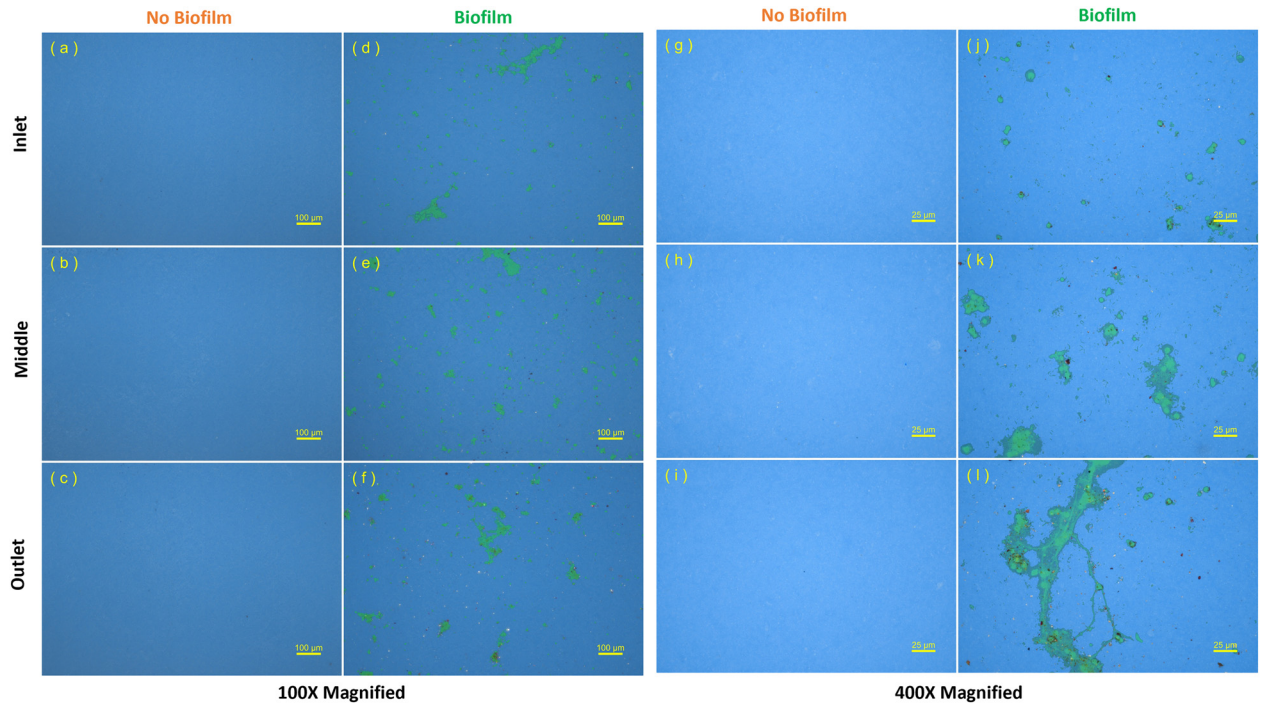

Fig. 3 Microscopy images of pipe wall samples collected from the biofilm and no-biofilm experiments before the particle injection phase, from the invert position of the pipes at the inlet, middle, and outlet pipe loop locations, at magnifications of 100× and 400×. Biofilm images (DNA-labelled in green) were overlayed on top of brightfield images that show the pipe wall surface in blue.

microbial cell morphologies were also identified in the corresponding fluorescent images (Fig. S7), suggesting the presence of a rich and diverse environment of microorganisms in the biofilm matrix.

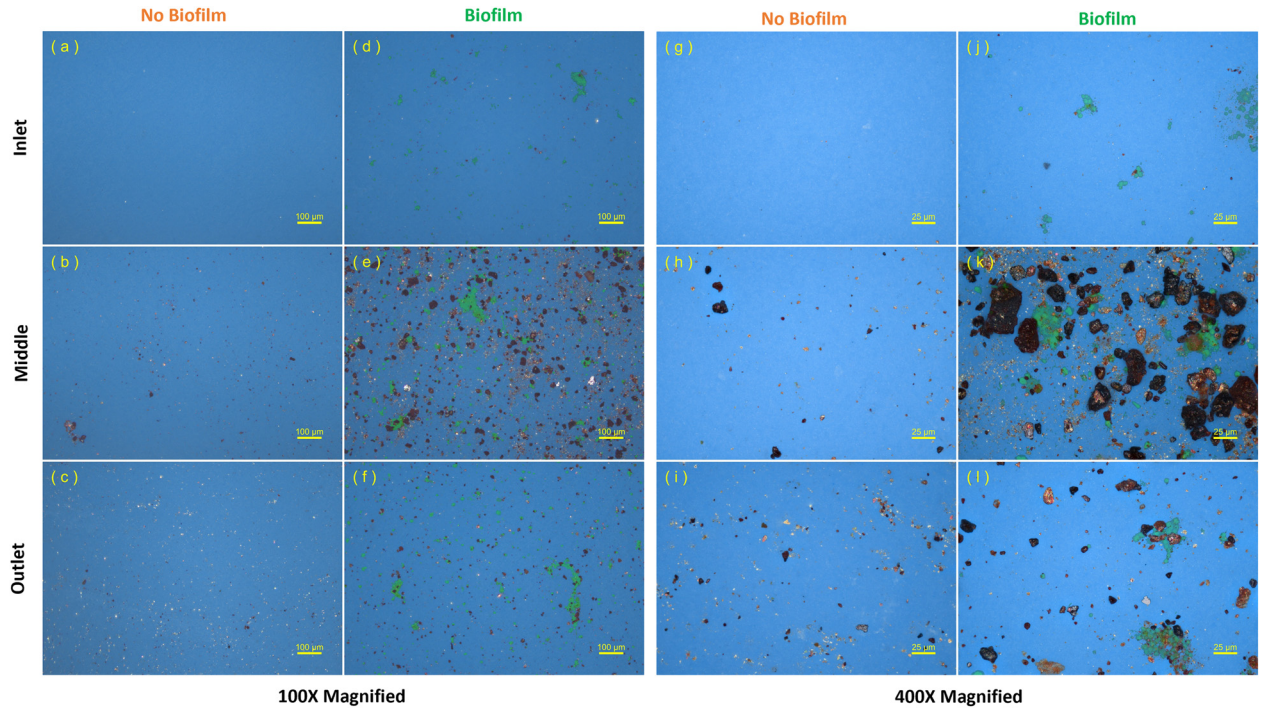

Fig. 4 Microscopy images of pipe wall samples collected from the biofilm and no-biofilm experiments after the particle injection phase, from the invert position of the pipes at the inlet, middle, and outlet pipe loop locations, at magnifications of 100× and 400×. Biofilm images (DNA-labelled in green) were overlayed on top of brightfield images that show the pipe wall surface in blue.

Pipe wall conditions after particle addition. Fig. 4 shows microscopy images from pipe samples collected after particle addition. Samples from the pipe inlet (upstream of the particle injection point – Fig. 1) did not encounter the particle plug and thus showed no particle attachment (Fig. 4a and d). Occasionally, a few particles were observed on samples taken at the inlet in the biofilm experiment. These were likely remnants from previous experiments in the pipe loop that were entrapped in the biofilm during the 28-day growth period.

Heavy iron oxide particle accumulation was observed on the pipe invert surfaces exposed to particle flow (Fig. 4b, c, e and f). The highest particle density occurred in the midpoint section of the biofilm experiment (Fig. 4e), where particles of various sizes were embedded in biofilm clusters. By comparison, fewer particles were present in the downstream section of the biofilm experiment (~86 m from injection – Fig. 1) at the outlet (Fig. 4f), where the largest and smallest particles seen in the midpoint section were absent. Higher-magnification images (Fig. 4k and 2l) confirm this size-based depletion, suggesting that small particles were retained along the pipe walls in the biofilm experiment. Particles as large as 30 μm were observed (Fig. 4k) in the biofilm experiment, which demonstrates that biofilm EPS facilitated the capture of large particles.

In the no-biofilm experiment, only smaller particles were observed (Fig. 4b and c). The absence of larger particles likely suggests insufficient adhesion without the presence of biofilms; these particles were probably removed during the washing step. At the midpoint position (Fig. 4b), some slightly larger particles were present, while the outlet (Fig. 4c) showed a higher concentration of fine particles. At a magnification of 400× (Fig. 4h and i), fewer fine particles were seen on the coupon samples taken at the midpoint (Fig. 4h) in comparison to the outlet (Fig. 4i), possibly due to a loss of particles during washing because of higher concentrations of loose particles. Notably, particle density varied substantially across fields of view (FOVs) from the same coupon samples taken in the no-biofilm experiment (see images mosaics available at SI). This was likely due to the surface tension forces acting on loose particles during pipe wall samples collection and washing.

Pipe wall conditions after flushing step F1. Fig. 5 presents microscopy images after the first flushing step (F1), which used the same flow direction as the particle attachment phase. Coupon samples taken at the inlet remained free of particles (Fig. 5a, d, g and j), as they were not exposed to the particle plug. For the no-biofilm experiment, the midpoint location showed a substantial reduction in attached particles post-flushing (Fig. 5b and h), as expected for loosely adhered particles. Conversely, the coupon samples at the outlet (Fig. 5c and i) showed no substantial particle loss after flushing. At 400×, larger particle clusters could be found in some FOVs (Fig. 5i) not previously seen at this location (Fig. 4i), suggesting particles reattachment during flushing step F1.

In the biofilm experiment, flushing reduced biofilm clusters, but many particles and biofilm clusters remained

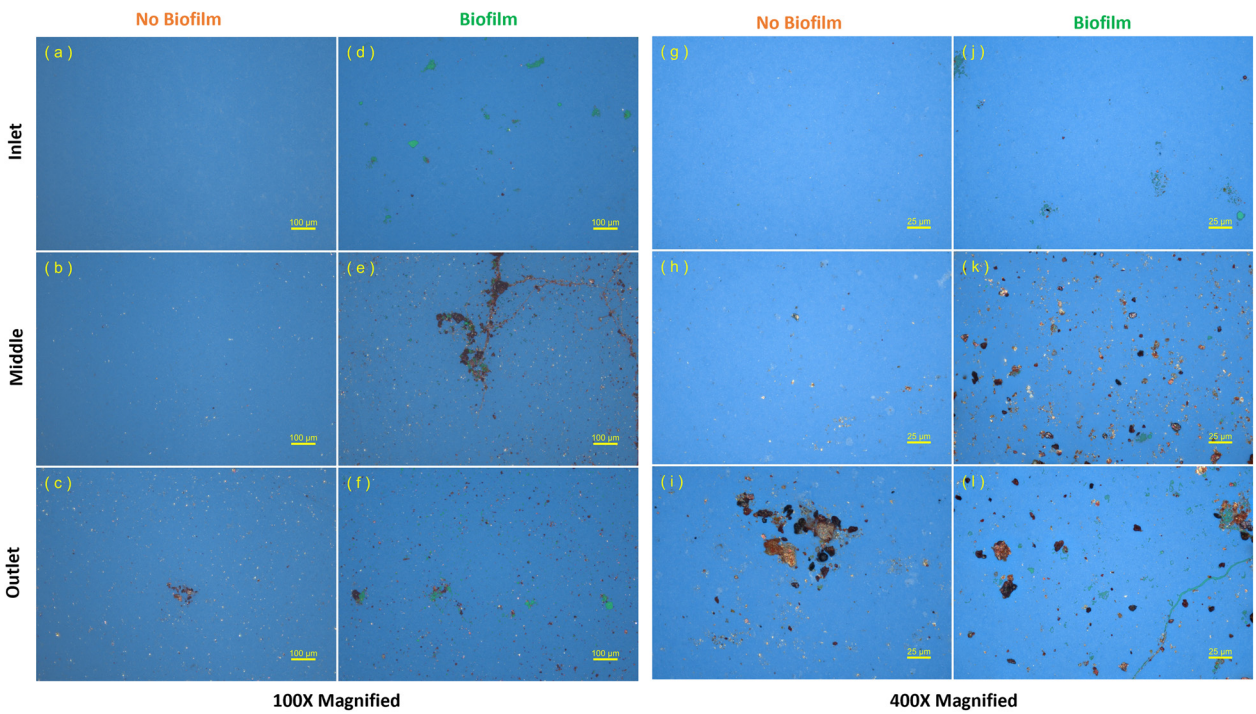

Fig. 5 Microscopy images of pipe wall samples collected from the biofilm and no-biofilm experiments after flushing step F1, from the invert position of the pipes at the inlet, middle, and outlet pipe loop locations, at magnifications of 100× and 400×. Biofilm images (DNA-labelled in green) were overlayed on top of brightfield images that show the pipe wall surface in blue.

attached (Fig. 5d–f). Some FOVs (*e.g.*, Fig. 5e and l) showed iron oxide clusters resembling earlier biofilm clusters (Fig. 3l), reinforcing the idea that biofilm EPS enhances particle adhesion and hinder mobilization. Even where biofilms were not visibly present through DNA staining, high numbers of large particles remained (Fig. 5k and l), suggesting that biofilm-secreted substances or unstained EPS may have modified pipe wall adhesion properties.[42] While SYTO9 marks DNA-rich biofilm components (*e.g.*, DNA in microbial cells and extra-cellular DNA in EPS), the chlorine content of the flushing water may have also reduced biofilm visibility in fluorescence images.

The persistence of particles in the biofilm experiment after flushing step F1 may also explain the substantial material release observed in subsequent flushes (F2–F4).

Discussion

Biofilm mechanisms of particle capture

Results from the particle attachment phase and from the FSS profiles of flushing step F1 (which highlights the pipe loop sections with greater particle accumulation) suggest that biofilms played an important role in promoting the attachment of iron oxide particles to the pipe wall. The data indicates that larger iron oxide particles were able to adhere to the biofilm-coated pipe walls, whereas they were only loosely deposited on the pipe wall in the no-biofilm experiment. This outcome is likely caused by biofilm EPS, which has notable adhesion properties and facilitates the attachment of particles to the pipe walls. Additionally, Fig. 4f and l show that fine particles were almost entirely removed from the particle suspension after passing through ~90 meters of pipe (Fig. 1) in the biofilm experiment, while they remained present in high concentrations in the no-biofilm experiment (Fig. 4c and i). This suggests that the attachment rate of fine particles (~1 μm) was substantially higher in the biofilm experiment. This observation also explains the consistent FSS values recorded between 60 and 120 seconds during the F1 flushing step of the biofilm experiment (Fig. 2a).

Nonetheless, comparisons between pipe wall samples from both experiments suggest that SSC, particle sizes, and pipe wall conditions all contributed to differences in particle attachment rates. These findings reinforce existing hypotheses regarding the role of pipe wall roughness and particle size in promoting attachment,[23,33] while also highlighting the importance of surface conditioning factors—such as biofilms—that can alter surface properties.

Furthermore, the relatively low DNA-stained biofilm coverage (~3%) observed in these experiments seems insufficient to fully account for the increased adhesion of both large and fine particles. Images from the biofilm experiment (Fig. 4e and f) show that most attached particles do not spatially correlate with visible biofilm clusters yet still adhere to the pipe wall. This suggests enhanced adhesive interactions between the pipe wall and particles in the biofilm experiment compared to the no-biofilm experiment. One possible explanation is that biofilm-forming microorganisms secrete molecular substances that "prime" surfaces, increasing their adhesiveness[42] and thereby strengthen the forces that retain particles on the pipe wall. These substances may include adhesins and surface conditioning molecules,[50,51] which are not labelled by SYTO9 used here. However, their role in enhancing particle attachment has yet to be confirmed. This hypothesis may help explain the increased adhesion rates of particles of all sizes, especially fine particles. At the same time, the absence of biofilms and particle deposits on the obvert (top) position of the pipes may indicate that the adhesive enhancement from surface-priming substances was still insufficient to overcome gravitational and shear forces, which together prevented material accumulation in those areas.

In contrast, fields of view (FOVs) showing a clear spatial correlation between particles and biofilm clusters were more frequently observed in images taken after the first flushing step – F1 (Fig. 5e and f). This suggests that some biofilm clusters can offer even stronger adhesion to particles and resist particle mobilization more effectively. Additionally, the higher SSC and turbulence intensity during high flow flushing increase the likelihood of suspended particles colliding with pipe walls. These collisions may raise the chance of particles encountering resistant biofilm clusters and re-attaching to their EPS at pipe surface during flushing. In such cases, a strong spatial correlation between particle re-attachment and biofilm presence is expected and observed in these experimental results.

Moreover, the adhesion forces between biofilm clusters and the pipe wall likely scale with the cluster EPS contact area (*i.e.*, how well they anchor to the surface), while the adhesion between particles and biofilms depends on the contact area between individual particles and the EPS. These interactions are expected to be substantially stronger than the minor enhancements proposed by the surface-coating hypothesis discussed earlier. Based on this, it is hypothesized that pipes with older, well-developed biofilms (*e.g.*, with a high surface area and potentially covering 100% of the inner pipe wall) will exhibit a much greater capacity for particle capture. In such cases, the adhesion properties of biofilms would far exceed those of particles attaching directly to pipe wall substrate. However, further experiments are needed to investigate pipes with extensive biofilm coverage and to confirm this hypothesis.

Turbidity *vs.* SSC

The quantification of materials that accumulate and detach from the pipe walls of drinking water distribution systems (DWDS) plays an important role in understanding contaminant dynamics in these systems. Researchers have long emphasized the lack of standardized methods for such assessments, particularly the limitations in translating turbidity measurements into suspended solids concentration

(SSC).[25,26] While turbidity is generally correlated with SSC, the precise conversion between the two depends on various factors, including the characteristics of suspended particles and the operational specifics of turbidimeters.[24]

In these experiments, turbidity-to-SSC conversion coefficients (α) ranged from 0.1 to 4.7 mg L^{-1} NTU^{-1}. Data from the particle injection step, representing particles directly injected in the pipe flow, confirmed previous findings of low α values between 0.1 and 0.2.[23] The values below 1 suggest that turbidity tends to overestimate SSC. In contrast, higher α values were observed during the mobilization phase, where particles were mobilized from pipe walls, indicating that turbidity underestimated SSC ($\alpha > 1$).

Interestingly, lower α values were recorded during the initial flushing steps (F1 and F2) of the biofilm experiment compared to the no-biofilm experiment. This suggests that the presence of biofilm can substantially affect α, even when inorganic sediments dominate. One possible explanation is that more particles accumulated and were subsequently mobilized along the entire length of the pipe loop in the biofilm experiment. This reduced the disparity between particles detached during the initial peak and those from other sections of the pipe. This would improve the ability of the coefficient α to more accurately represent the true SSC across the entire flush volume in the biofilm experiment. Alternatively, organic substances released from the biofilm may have altered the optical properties of suspended particles and form larger particles by clustering fine sediments, thereby affecting turbidity readings.

As discussed in the results section, the imbalance in the total mass of material accumulated and mobilized from pipes during this experiment is likely due to an unstable α value during the F1 flushing step. The FSS peaks in Fig. 2a correspond to the mobilization of large particles that quickly settle after injection and account for a substantial portion of the mobilized mass. However, these peaks are not well-represented in the flushing samples, which were designed to avoid collecting the diluted water immediately following the peaks. Higher-resolution SSC sampling during flushing step F1 would have been ideal for capturing variations in the α coefficient but would have required much higher sampling flow rates to ensure SSC could be detected in the collected samples.

Additionally, in these experiments, all samples and turbidity data were collected from sampling tubes located at the pipe centerline, aligned with the flow direction. This configuration was chosen to minimize interference from pipe walls or sudden flow direction changes at the sampling ports. However, this setup may have overlooked bed-flow transport of larger particles that are not easily suspended. The transport and behavior of larger particles in DWDSs remain active areas of research, and further studies are needed to clarify their influence on turbidity measurements.

Overall, our results underscore the challenges of quantifying materials in DWDSs. We strongly recommend that researchers interpret turbidity data with caution and prioritize SSC measurements when attempting to quantify material in physical units (mg). Future research would greatly benefit from standardizing material load units and improving the accuracy and quality of such estimations.

Experimental limitations

The experimental results presented here were obtained under specific laboratory conditions and therefore have several limitations, discussed below. The aim was to investigate specific mechanisms of drinking water discoloration by isolating variables within a DWDS. As such, these results do not represent the full range of conditions found in DWDSs and extrapolating them should be done with consideration of the specific context of other systems.

Hydraulic limitations. During the biofilm growth and particle injection steps, the experimental pipe loop operated under a steady flow rate of 0.6 L s^{-1} and a pressure of 280 kPa (Table 1). While this flow rate corresponds to an average flow found in a typical distribution pipe in North American systems, the steady-state condition was selected to simplify biofilm development and particle accumulation processes. However, such steady flow is not representative of typical operational DWDSs.

In real networks, flow patterns typically vary throughout the day, with peak flows occurring during high-demand hours and low flows at night. These fluctuations are known to influence material accumulation and discoloration behavior.[48] Accumulation is often simulated with the daily peak flow rate, which is typically higher than the flow used in this study. Consequently, in real systems, materials with adhesion forces below the WSS that correspond to the peak flow are typically mobilized, meaning that only more strongly adhering materials accumulate on pipes. This leads to higher resistance to mobilization in operational DWDSs.[17]

Additionally, biofilms respond to flow variation, adapting their adhesion and cohesion in accordance with WSS.[39] The steady flow in this experiment likely resulted in biofilms with lower cohesion and adhesion, contributing to the development of a less dense structure that was more easily mobilized during flushing.

Future experiments incorporating variable flow conditions are needed to validate these findings and improve their applicability to operational DWDSs.

Biofilm growth limitations. In the experiments, biofilms were developed and grown with microorganisms found in the local drinking water. Moreover, the conditions imposed on the biofilms to accelerate their growth are not usually found in DWDSs. Methods used to harvest and concentrate microbial communities may have introduced selection biases. Furthermore, the absence of disinfectants and the presence of additional nutrients during the biofilm growth do not reflect the conditions of North American drinking water systems. This likely influenced the microbial community composition of the resulting biofilms and their EPS properties.

The rapid inoculation of a high-concentration solution of microorganisms at the start of pre-conditioning step may have led to dominant biofilm growth on the invert (bottom) of the pipe. It is hypothesized that floating biofilm clusters in the inoculated solution were too large to attach to the obvert (top) surface of the pipe, possibly due to gravitational forces. In contrast, biofilms in operational DWDSs are reported to grow along the entire pipe circumference,[7,46] although it remains unclear whether this distribution is a result of extended growth periods or if biomass can substantially differ between pipe invert and obvert positions.

Methods used to visualize biofilms through DNA-labeling fluorescence staining also have limited capacity to detect other biofilm components. Carbohydrates and proteins that lack DNA are not visible using this method and are likely present within our biofilms.[34]

Particle limitations. Ferric iron particles were selected for these experiments to simulate those found during discoloration events in DWDSs. These particles were chosen for their insolubility and size resemblance to particles derived from cast iron corrosion. However, their composition is limited when compared to the broader range of corrosion scales found in DWDSs,[52] and the fixed particle size distribution may not accurately reflect what has been observed in discoloration events.[32]

In operational systems, particles from corrosion often contain various iron oxides/hydroxides (*e.g.*, $Fe(OH)_2$, $Fe(OH)_3$, FeOOH), which can dissociate or re-flocculate depending on water chemistry, making their concentration and size distribution less predictable.

Additionally, the method of injecting particles at the centerline of the pipe loop at the midpoint of the pipe loop does not fully replicate how suspended particles behave in DWDSs. Larger injected particles were observed to settle quickly, forming a loose deposit that caused the FSS peaks seen in flushing step F1 (Fig. 2a). While similar patterns of accumulation may occur in corroding metal pipes, it is unlikely that such loose deposits form as readily in PVC pipes. Due to the lack of field data, it remains difficult to define what constitutes 'typical particle accumulation' in plastic pipe mains.

Conclusions

This study demonstrated that biofilms substantially influence the accumulation and mobilization of iron oxide particles in drinking water distribution systems. The presence of biofilms increased particle attachment to pipe walls by 6%, raising total retention from 66% to 72%. Additionally, biofilms enhanced the resistance of attached particles to mobilization, as reflected by a 7% lower release of material during the initial flushing step compared to pipes without biofilms. Microscopy confirmed that biofilm EPS enabled both fine and large particles to adhere more uniformly along the pipe length, including particles that otherwise remained in suspension or were loosely attached in the no-biofilm experiment.

Subsequent flushing showed that biofilm-coated pipes retained a larger proportion of material, requiring higher wall shear stresses (WSS) for effective mobilization. Notably, particles mobilized from biofilm conditions also included a greater fraction of organic matter, indicating biofilm disruption during flushing.

These findings underscore the dual role of biofilm EPS in promoting particle capture and hindering their removal, with implications for discoloration risk and hydraulic maintenance. Importantly, the variability in turbidity-to-SSC conversion coefficients further highlights the need for direct SSC measurements to accurately quantify material loads. This work emphasizes the necessity of incorporating biofilm-particle dynamics into management strategies for maintaining water quality in distribution networks. Future experiments should explore biofilm-particle interactions under more realistic and variable flow conditions, including older and more developed biofilms representative of operational DWDS.

Author contributions

Conceptualization: A. S. B., Y. F.; methodology: A. S. B., Y. F., B. A.; investigation: A. S. B., B. A.; resources: A. S. B., Y. F.; writing: A. S. B., Y. F.; visualization: A. S. B.; supervision: Y. F.; project administration: Y. F.; funding acquisition: Y. F.

Conflicts of interest

There are no conflicts to declare.

Data availability

The main data supporting the findings of this study are included within the manuscript. Additional data is available in 1) the supplementary information (SI) file; and 2) a data repository containing the complete dataset of microscopy images used in this investigation: https://doi.org/10.5683/SP3/UQZLFH.

Supplementary information is available. See DOI: https://doi.org/10.1039/d5ew00913h.

References

1 J. Boxall, M. Blokker, P. Schaap, V. Speight and S. Husband, Managing discolouration in drinking water distribution systems by integrating understanding of material behaviour, *Water Res.*, 2023, **243**, 120416, DOI: 10.1016/j.watres.2023.120416.
2 J. H. Vreeburg and J. B. Boxall, Discolouration in potable water distribution systems: a review, *Water Res.*, 2007, **41**(3), 519–529, DOI: 10.1016/j.watres.2006.09.028.
3 L. S. McNeill and M. Edwards, Iron pipe corrosion in distribution systems, *J. AWWA*, 2001, **93**(7), 88–100, DOI: 10.1002/j.1551-8833.2001.tb09246.x.

4 P. Sarin, J. A. Clement, V. L. Snoeyink and W. M. Kriven, Iron Release from corroded, unlined cast-iron pipe, *J. - Am. Water Works Assoc.*, 2003, **95**(11), 85–96, (acccessed 2022/02/13/). JSTOR.
5 D. M. Cook and J. B. Boxall, Discoloration Material Accumulation in Water Distribution Systems, *J. Pipeline Syst. Eng. Pract.*, 2011, **2**(4), 113–122, DOI: 10.1061/(asce)ps.1949-1204.0000083.
6 P. S. Husband and J. B. Boxall, Asset deterioration and discolouration in water distribution systems, *Water Res.*, 2011, **45**(1), 113–124, DOI: 10.1016/j.watres.2010.08.021.
7 S. Husband, K. E. Fish, I. Douterelo and J. Boxall, Linking discolouration modelling and biofilm behaviour within drinking water distribution systems, *Water Supply*, 2016, **16**(4), 942–950, DOI: 10.2166/ws.2016.045, (acccessed 2/17/2022).
8 G. Liu, Y. Tao, Y. Zhang, M. Lut, W. J. Knibbe, P. van der Wielen, W. Liu, G. Medema and W. van der Meer, Hotspots for selected metal elements and microbes accumulation and the corresponding water quality deterioration potential in an unchlorinated drinking water distribution system, *Water Res.*, 2017, **124**, 435–445, DOI: 10.1016/j.watres.2017.08.002.
9 J. Liu, H. Chen, L. Yao, Z. Wei, L. Lou, Y. Shan, S. D. Endalkachew, N. Mallikarjuna, B. Hu and X. Zhou, The spatial distribution of pollutants in pipe-scale of large-diameter pipelines in a drinking water distribution system, *J. Hazard. Mater.*, 2016, **317**, 27–35, DOI: 10.1016/j.jhazmat.2016.05.048.
10 S. Gholipour, Z. Shamsizadeh, W. Gwenzi and M. Nikaeen, The bacterial biofilm resistome in drinking water distribution systems: A systematic review, *Chemosphere*, 2023, **329**, 138642, DOI: 10.1016/j.chemosphere.2023.138642.
11 I. M. Oliveira, I. B. Gomes, L. C. Simões and M. Simões, A review of research advances on disinfection strategies for biofilm control in drinking water distribution systems, *Water Res.*, 2024, **253**, 121273, DOI: 10.1016/j.watres.2024.121273.
12 C. Margot, W. Rhoads, M. Gabrielli, M. Olive and F. Hammes, Dynamics of drinking water biofilm formation associated with Legionella spp. colonization, *npj Biofilms Microbiomes*, 2024, **10**(1), 101, DOI: 10.1038/s41522-024-00573-x.
13 P. W. J. J. van der Wielen, M. Dignum, A. Donocik and E. I. Prest, Influence of Temperature on Growth of Four Different Opportunistic Pathogens in Drinking Water Biofilms, *Microorganisms*, 2023, **11**(6), 1574.
14 B. A. Hemdan, G. E. El-Taweel, P. Goswami, D. Pant and S. Sevda, The role of biofilm in the development and dissemination of ubiquitous pathogens in drinking water distribution systems: an overview of surveillance, outbreaks, and prevention, *World J. Microbiol. Biotechnol.*, 2021, **37**(2), 36, DOI: 10.1007/s11274-021-03008-3.
15 C. C. Preciado, J. Boxall, V. Soria-Carrasco, S. Martínez and I. Douterelo, Implications of Climate Change: How Does Increased Water Temperature Influence Biofilm and Water Quality of Chlorinated Drinking Water Distribution Systems?, *Front. Microbiol.*, 2021, **12**, DOI: 10.3389/fmicb.2021.658927.
16 S. Husband, J. Mistry and J. Boxall, Modelling and Flow Conditioning to Manage Discolouration in Trunk Mains, *Procedia Eng.*, 2014, **70**, 833–842, DOI: 10.1016/j.proeng.2014.02.091.
17 W. R. Furnass, R. P. Collins, P. S. Husband, R. L. Sharpe, S. R. Mounce and J. B. Boxall, Modelling both the continual erosion and regeneration of discolouration material in drinking water distribution systems, *Water Supply*, 2014, **14**(1), 81–90, DOI: 10.2166/ws.2013.176.
18 J. van Summeren and M. Blokker, Modeling particle transport and discoloration risk in drinking water distribution networks, *Drinking Water Eng. Sci.*, 2017, **10**(2), 99–107, DOI: 10.5194/dwes-10-99-2017.
19 J. B. Boxall and A. J. Saul, Modeling Discoloration in Potable Water Distribution Systems, *J. Environ. Eng.*, 2005, **131**(5), 716–725, DOI: 10.1061/(ASCE)0733-9372(2005)131:5(716).
20 W. Furnass, I. Douterelo, R. Collins, S. Mounce and J. Boxall, Controlled, Realistic-scale, Experimental Study of How the Quantity and Erodibility of Discolouration Material Varies with Shear Strength, *Procedia Eng.*, 2014, **89**, 135–142, DOI: 10.1016/j.proeng.2014.11.169.
21 S. Husband, M. Jackson and J. Boxall, Identifying Material Accumulation Processes in Drinking Water Distribution Systems with Extended Period EPANET MSX Turbidity Simulations, *Procedia Eng.*, 2015, **119**, 398–406, DOI: 10.1016/j.proeng.2015.08.901.
22 S. Husband and J. B. Boxall, Field Studies of Discoloration in Water Distribution Systems: Model Verification and Practical Implications, *J. Environ. Eng.*, 2010, **136**(1), 86–94, DOI: 10.1061/(asce)ee.1943-7870.0000115.
23 A. S. Braga and Y. Filion, The interplay of suspended sediment concentration, particle size and fluid velocity on the rapid deposition of suspended iron oxide particles in PVC drinking water pipes, *Water Res.: X*, 2022, **15**, 100143, DOI: 10.1016/j.wroa.2022.100143.
24 B. G. B. Kitchener, J. Wainwright and A. J. Parsons, A review of the principles of turbidity measurement, *Prog. Phys. Geogr.*, 2017, **41**(5), 620–642, DOI: 10.1177/0309133317726540.
25 A. Rymszewicz, J. J. O'Sullivan, M. Bruen, J. N. Turner, D. M. Lawler, E. Conroy and M. Kelly-Quinn, Measurement differences between turbidity instruments, and their implications for suspended sediment concentration and load calculations: A sensor inter-comparison study, *J. Environ. Manage.*, 2017, **199**, 99–108, DOI: 10.1016/j.jenvman.2017.05.017.
26 T. Walski, K. Minnich, C. Sherman, L. Strause and B. Whitman, Can There be a Law of Conservation of Turbidity, *Procedia Eng.*, 2017, **186**, 372–379, DOI: 10.1016/j.proeng.2017.03.233.
27 J. Boxall, I. Douterelo, K. E. Fish and S. Husband, Linking discolouration modelling and biofilm behaviour within drinking water distribution systems, *Water Supply*, 2016, **16**(4), 942–950, DOI: 10.2166/ws.2016.045.
28 H. Armand, I. I. Stoianov and N. J. D. Graham, A holistic assessment of discolouration processes in water distribution

networks, *Urban Water J.*, 2015, **14**(3), 263–277, DOI: 10.1080/1573062x.2015.1111912.

29 J. Verberk, J. H. G. Vreeburg, L. C. Rietveld and J. C. van Dijk, Particulate fingerprinting of water quality in the distribution system, *Water S.A.*, 2009, **35**, 192–199.

30 J. H. Vreeburg, D. Schippers, J. Q. Verberk and J. C. van Dijk, Impact of particles on sediment accumulation in a drinking water distribution system, *Water Res.*, 2008, **42**(16), 4233–4242, DOI: 10.1016/j.watres.2008.05.024.

31 A. S. Braga and Y. Filion, Initial stages of particulate iron oxide attachment on drinking water PVC pipes characterized by turbidity data and brightfield microscopy from a full-scale laboratory, *Environ. Sci.: Water Res. Technol.*, 2022, **8**, 1195–1210, DOI: 10.1039/D2EW00010E.

32 J. B. Boxall, A. J. Saul, J. D. Gunstead and N. Dewis, Regeneration of Discolouration in Distribution Systems, in *World Water & Environmental Resources Congress 2003*, 2003, pp. 1–9.

33 A. Sass Braga and Y. Filion, Examining the conditioning factors that influence material shear strength of particle deposits in a full-scale drinking water distribution laboratory, *Environ. Sci.: Water Res. Technol.*, 2023, **9**(10), 2619–2630, DOI: 10.1039/D3EW00159H.

34 K. E. Fish, A. M. Osborn and J. Boxall, Characterising and understanding the impact of microbial biofilms and the extracellular polymeric substance (EPS) matrix in drinking water distribution systems, *Environ. Sci.: Water Res. Technol.*, 2016, **2**(4), 614–630, DOI: 10.1039/c6ew00039h.

35 M. J. Lehtola, T. K. Nissinen, I. T. Miettinen, P. J. Martikainen and T. Vartiainen, Removal of soft deposits from the distribution system improves the drinking water quality, *Water Res.*, 2004, **38**(3), 601–610, DOI: 10.1016/j.watres.2003.10.054.

36 B. Barbeau, K. Julienne, A. Carriere and V. Gauthier, Dead-end flushing of a distribution system: Short and long-term effects on water quality, *J. Water Supply: Res. Technol.–AQUA*, 2005, **54**(6), 371–383, DOI: 10.2166/aqua.2005.0035.

37 A. Carrière, V. Gauthier, R. Desjardins and B. Barbeau, Evaluation of loose deposits in distribution systems through: unidirectional flushing, *J. - Am. Water Works Assoc.*, 2005, **97**(9), 82–92, DOI: 10.1002/j.1551-8833.2005.tb07474.x.

38 C. Farrell, F. Hassard, B. Jefferson, T. Leziart, A. Nocker and P. Jarvis, Turbidity composition and the relationship with microbial attachment and UV inactivation efficacy, *Sci. Total Environ.*, 2018, **624**, 638–647, DOI: 10.1016/j.scitotenv.2017.12.173.

39 K. Fish, A. M. Osborn and J. B. Boxall, Biofilm structures (EPS and bacterial communities) in drinking water distribution systems are conditioned by hydraulics and influence discolouration, *Sci. Total Environ.*, 2017, **593-594**, 571–580, DOI: 10.1016/j.scitotenv.2017.03.176.

40 S. Liu, C. Gunawan, N. Barraud, S. A. Rice, E. J. Harry and R. Amal, Understanding, Monitoring, and Controlling Biofilm Growth in Drinking Water Distribution Systems, *Environ. Sci. Technol.*, 2016, **50**(17), 8954–8976, DOI: 10.1021/acs.est.6b00835.

41 H. C. Flemming, J. Wingender, U. Szewzyk, P. Steinberg, S. A. Rice and S. Kjelleberg, Biofilms: an emergent form of bacterial life, *Nat. Rev. Microbiol.*, 2016, **14**(9), 563–575, DOI: 10.1038/nrmicro.2016.94.

42 H. C. Flemming and J. Wingender, The biofilm matrix, *Nat. Rev. Microbiol.*, 2010, **8**(9), 623–633, DOI: 10.1038/nrmicro2415.

43 American Water Works Association, *Standard Methods for the Examination of Water and Wastewater, Section 2540 D: Total Suspended Solids*, APHA Press, 2023.

44 B. Anderson, A. Sass Braga, Y. Filion and S. J. Payne, Behaviour of particle mobilization and reattachment under flushing conditions in PVC pipes using a full-scale laboratory system, *Environ. Sci.: Water Res. Technol.*, 2025, **11**(3), 714–724, DOI: 10.1039/D4EW00764F.

45 A. S. Braga and Y. Filion, A novel monitoring scheme to detect iron oxide particle deposits on the internal surface of PVC drinking water pipes, *Environ. Sci.: Water Res. Technol.*, 2021, **7**(11), 2116–2128, DOI: 10.1039/D1EW00614B.

46 K. E. Fish, R. Collins, N. H. Green, R. L. Sharpe, I. Douterelo, A. M. Osborn and J. B. Boxall, Characterisation of the physical composition and microbial community structure of biofilms within a model full-scale drinking water distribution system, *PLoS One*, 2015, **10**(2), e0115824, DOI: 10.1371/journal.pone.0115824.

47 A. S. Braga, R. Saulnier, Y. Filion and A. Cushing, Dynamics of material detachment from drinking water pipes under flushing conditions in a full-scale drinking water laboratory system, *Urban Water J.*, 2020, **17**(8), 745–753, DOI: 10.1080/1573062x.2020.1800759.

48 P. S. Husband, J. B. Boxall and A. J. Saul, Laboratory studies investigating the processes leading to discolouration in water distribution networks, *Water Res.*, 2008, **42**(16), 4309–4318, DOI: 10.1016/j.watres.2008.07.026.

49 R. L. Sharpe, C. J. Smith, J. B. Boxall and C. A. Biggs, Pilot Scale Laboratory Investigations into the Impact of Steady State Conditioning Flow on Potable Water Discolouration. in *Water Distribution Systems Analysis 2010*, 2011, pp. 494–506.

50 Y. Cheng, G. Feng and C. I. Moraru, Micro- and Nanotopography Sensitive Bacterial Attachment Mechanisms: A Review, *Front. Microbiol.*, 2019, **10**, DOI: 10.3389/fmicb.2019.00191.

51 C. Berne, A. Ducret, G. G. Hardy and Y. V. Brun, Adhesins Involved in Attachment to Abiotic Surfaces by Gram-Negative Bacteria, *Microbiol. Spectrum*, 2015, **3**(4), DOI: 10.1128/microbiolspec.mb-0018-2015.

52 A. S. Benson, A. M. Dietrich and D. L. Gallagher, Evaluation of Iron Release Models for Water Distribution Systems, *Crit. Rev. Environ. Sci. Technol.*, 2012, **42**(1), 44–97, DOI: 10.1080/10643389.2010.498753.

53 U. Waqas, A. Farhan, A. Haider, U. Qumar and A. Raza, Advancements in biofilm formation and control in potable water distribution systems: A comprehensive review and analysis of chloramine decay in water systems, *J. Environ. Chem. Eng.*, 2023, **11**(6), DOI: 10.1016/j.jece.2023.111377.

54 I. Douterelo, M. Jackson, C. Solomon and J. Boxall, Microbial analysis of in situ biofilm formation in drinking water distribution systems: implications for monitoring and control of drinking water quality, *Appl. Microbiol. Biotechnol.*, 2016, **100**, 3301–3311, DOI: 10.1007/s00253-015-7155-3.